Linear and Non-linear Geometric Object Matching with Implicit Representation

Alex Leow[1], Ming-Chang Chiang[1], Hillary Protas[2], Paul Thompson[1], Luminita Vese[3], and Henry S.C. Huang[2]

[1]Laboratory of Neuroimaging, [2]Department of Biomathematics, and [3]Department of Mathematics

University of California, Los Angeles

E-mail (Alex Leow): alexiadleow@yahoo.com

Abstract

This paper deals with the matching of geometric objects including points, curves, surfaces, and subvolumes using implicit object representations in both linear and non-linear settings. This framework can be applied to feature-based non-linear image warping in biomedical imaging with the deformation constrained to be one-to-one, onto, and diffeomorphic. Moreover, a theoretical connection is established between the well known Hausdorff metric and the framework proposed in this paper. A general strategy for matching geometric objects in both 2D and 3D is discussed. The corresponding Euler-Lagrange equations are presented and gradient descent method is employed to solve the time dependent partial differential equations.

1. Introduction

Object comparison is a challenging problem in computer vision, image processing, pattern recognition, statistics, artificial intelligence, and many other scientific fields. Shape, by far the most common geometric concept encountered in object comparison, plays an important role in both theory and application. A fundamental problem in shape comparison is shape matching, in which one shape is matched to other shapes by minimizing a dissimilarity measure.

In this paper, we introduce an unifying approach for matching general geometric patterns such as point sets, curves, surfaces, and regions in both 2D and 3D using an implicit representation based on the level set method. This approach offers a new perspective in terms of how the geometric patterns are formulated mathematically and provides a flexible framework for both rigid and non-rigid object matching.

2. Implicit representation of objects

Traditionally in computer science, a shape is represented by a set of points that discretizes the contour of the shape. This approach has led to a large number of techniques for shape comparison based on matching the discretized point sets. In this paper, we take a different view by viewing geometric objects as the level contours of some functions defined on the whole image.

2.1. Implicit representation of shapes

Since the introduction of the level set method [1], implicit representation of shapes has been investigated extensively in the image processing community. In short, the closed contour of a shape can be represented by the zero level set of a level set function defined on the image. Though in theory, any level set function can be used for implicit representation, computationally it is often desirable that the level set function is the signed distance function to its zero level set. In this paper, we will assign positive values for areas inside the shape in the corresponding level set function.

2.2. Implicit representation of open curves

In order to represent an open curve C in 2D using level set functions, we follow the idea in [2] by extending C to a closed curve (represented by the zero level set of φ_1), and we further define a second closed curve (represented by the zero level set of φ_2), which encloses C and crosses the zero level set of φ_1 only at the end points of C. Then the open curve C can be written in the following way

$$C = \{x \mid \varphi_1(x) = 0,\ \varphi_2(x) > 0\}. \quad (1)$$

As for open curves in 2D, the representation for an open surface in 3D requires also the intersection of two level set functions in 3D. By the same argument, an open curve in 3-dimensional space can be represented by the intersection of three level set functions

$$C = \{x \mid \varphi_1(x) = 0,\ \varphi_2(x) = 0,\ \varphi_3(x) > 0\}. \quad (2)$$

2.3. Implicit representation of points

Though not well known, it is also possible to represent points using the intersection of level set

Proceedings of the 17th International Conference on Pattern Recognition (ICPR'04)
1051-4651/04 $ 20.00 IEEE

functions. For example, given two level set functions φ_1, φ_2 in 2D, the intersections of their zero level sets x_i, and any continuous function F, the following equation holds

$$F\delta(\varphi_1)\delta(\varphi_2)|\nabla\varphi_1\times\nabla\varphi_2|dx = \sum_i F(x_i)\cdot \quad (3)$$

The values of a function F at the intersections of the zero level sets of φ_1 and φ_2 could be recovered by an integral involving level set functions φ_1 and φ_2. This allows incorporation of point constraints into other variational formulations. Notice in 3D the left hand side of equation (3) evaluates the (closed) curve length of the intersection of 3D level set functions φ_1 and φ_2.

Similarly, given three level set functions in 3D with similar notations as in 2D, we have

$$F\delta(\varphi_1)\delta(\varphi_2)\delta(\varphi_3)|\nabla\varphi_1\times\nabla\varphi_2\cdot\nabla\varphi_2|dx = \sum_i F(x_i)\cdot \quad (4)$$

3. Theory

In object comparison, people are usually interested in matching with respect to certain equivalent classes. The equivalence class of an object is often defined as the invariance class of objects subject to group actions such as translation, rotation, and scaling. The level set method can be easily adapted to take equivalence classes into account. To this end, assuming a level set function ϕ is the signed distance function of its zero level set, then the following transformed level set function is still the signed distance function to its zero level set

$$\tilde{\phi} = r\phi\ \frac{(x-a)\cos\theta+(y-b)\sin\theta}{r}, \frac{-(x-a)\sin\theta+(y-b)\cos\theta}{r}. \quad (5)$$

In [3], the authors registered shapes by comparing their corresponding signed distance functions. In order to compare the distance functions independent of the size of the image, the authors proposed to compare only a narrow band near the zero level set. However, this approach usually requires a pre-processing to align the two shapes before registration by matching the centers of mass, for example. This approach fails when the shapes are far apart and the narrow bands do not overlap as no descent direction can be determined.

In this paper, we propose a different and more general strategy that can be utilized for objects of all types. Moreover, exact matching is achieved when the proposed cost function is zero. Thus, both comparison and exact matching are possible under this framework.

3.1. Overlapping shape matching

A different, yet widely used approach other than [3] for matching overlapping shapes in any dimension is to minimize the symmetric difference of the two level set functions. If the shapes are represented by the zero level set of ϕ and ψ, then the abovementioned approach boils down to solving for the translation-rotation-scaling parameters a, b, r, and θ such that under this transformation (as shown in equation (5)) the following cost function is minimized:

$$\min_{a,b,r,\theta}\int\{H(\tilde{\phi})(1-H(\psi))+H(\psi)(1-H(\tilde{\phi}))\}dx\cdot \quad (6)$$

Here H is the Heaviside function.

It is straightforward to see that this cost function is zero when these two shapes can be exactly registered. When minimizing this cost function, we need the derivative of the cost function with respect to $\tilde{\phi}$

$$\frac{\partial F}{\partial\tilde{\phi}} = (1-2H(\psi))\delta(\tilde{\phi})\cdot \quad (7)$$

3.2. Non-overlapping shape matching

The above cost function does not work for non-overlapping shapes as no gradient descent direction can be obtained. To overcome this, we could incorporate distance information into the cost function. Assuming level set functions ϕ and ψ are the signed distance function to their zero level sets, we look at the following modified cost function instead.

$$\min_{a,b,r,\theta}\int\{-\psi H(\tilde{\phi})(1-H(\psi))-\tilde{\phi}H(\psi)(1-H(\tilde{\phi}))\}dx\cdot \quad (8)$$

The derivative of the cost function with respect to $\tilde{\phi}$ is

$$\frac{\partial F}{\partial\tilde{\phi}} = -H(\psi)\{1-H(\tilde{\phi})-\delta(\tilde{\phi})\tilde{\phi}\}+\psi(1-H(\psi))\delta(\tilde{\phi}). \quad (9)$$

In short, we integrate $-\phi$ in the area: $\psi>0$, $\phi<0$, and integrate $-\psi$ in the area: $\psi<0$, $\phi>0$ and sum up the two integrals. Thus, this cost function is also non-negative and zero only when the shapes can be exactly registered. Moreover, since we are integrating the distance function to the shape, we always have gradient descent information wherever the initial position is.

3.3. Open curve matching

The above discussion on non-overlapping shapes helps us design cost functions for objects of any kind. Let us turn to the case of open curves, and construct the cost function by calculating the sum of line integrals on these two curves with respect to the other curve's distance function. Let us assume the two open curves C and C' of interest are represented by level set functions ϕ_1, ϕ_2 and ψ_1, ψ_2 respectively as in (1). Moreover, let us denote the distance functions of C and C' by $D_\phi(x)$ and $D_\psi(x)$. We now look at the following cost function:

$$\min_{a,b,r,\theta}\int\{\widetilde{D}_\phi\delta(\psi_1)|\nabla\psi_1|H(\psi_2)+D_\psi\delta(\tilde{\phi}_1)|\nabla\tilde{\phi}_1|H(\tilde{\phi}_2)\}dx\cdot \quad (10)$$

As before, we calculate the following

$$\frac{\partial F}{\partial \widetilde{\phi}_1} = -\frac{\delta_1}{\left|\partial \widetilde{\phi}_1\right|}\left\{H_2\left\langle \nabla D_\psi, \nabla \widetilde{\phi}_1 \right\rangle + D_\psi \delta_2 \left\langle \nabla \widetilde{\phi}_1, \nabla \widetilde{\phi}_1 \right\rangle\right\} - \delta_1 D_\psi H_2 div\left(\frac{\nabla \widetilde{\phi}_1}{\left|\nabla \widetilde{\phi}_1\right|}\right); \tag{11}$$

$$\frac{\partial F}{\partial \widetilde{\phi}_2} = D_\psi \delta_1 \delta_2 \left|\nabla \widetilde{\phi}_1\right| \nabla \widetilde{\phi}_2; \tag{12}$$

$$\frac{\partial F}{\partial \widetilde{D}_\phi} = \delta(\psi_1) H(\psi_2) \left|\nabla \psi_1\right|. \tag{13}$$

Here $\delta_1 = \delta(\widetilde{\phi}_1)$, $\delta_2 = \delta(\widetilde{\phi}_2)$, and $H_2 = H(\widetilde{\phi}_2)$.

Let us consider one more example, namely, closed curves in 3D. Assuming that one closed curve is represented by the intersection of ϕ_1, ϕ_2 and its distance function $D_\phi(x)$ with ψ_1, ψ_2, and $D_\psi(x)$ similarly defined for the other closed curve, we can consider the following cost function:

$$\min_{a,b,r\theta} \begin{matrix} \widetilde{D}_\phi \delta(\psi_1)\delta(\psi_2)\left|\nabla \psi_1 \times \nabla \psi_2\right| dx \\ + \; D_\psi \delta(\widetilde{\phi}_1)\delta(\widetilde{\phi}_2)\left|\nabla \widetilde{\phi}_1 \times \nabla \widetilde{\phi}_2\right| dx \end{matrix}. \tag{14}$$

The partial derivatives of this cost function are

$$\frac{\partial F}{\partial \widetilde{\phi}_1} = -div\left(\frac{P_{\nabla \widetilde{\phi}_2} \nabla \widetilde{\phi}_1}{\left|P_{\nabla \widetilde{\phi}_2} \nabla \widetilde{\phi}_1\right|}\left|\nabla \widetilde{\phi}_2\right| D_\psi\right)\delta(\widetilde{\phi}_1)\delta(\widetilde{\phi}_2); \tag{15}$$

$$\frac{\partial F}{\partial \widetilde{\phi}_2} = -div\left(\frac{P_{\nabla \widetilde{\phi}_1} \nabla \widetilde{\phi}_2}{\left|P_{\nabla \widetilde{\phi}_1} \nabla \widetilde{\phi}_2\right|}\left|\nabla \widetilde{\phi}_1\right| D_\psi\right)\delta(\widetilde{\phi}_1)\delta(\widetilde{\phi}_2); \tag{16}$$

$$\frac{\partial F}{\partial \widetilde{D}_\phi} = \delta(\psi_1)\delta(\psi_2)\left|\nabla \psi_1 \times \nabla \psi_2\right|. \tag{17}$$

Here the projection operator P acting on a vector v is

$$P_v = I - \frac{v \otimes v}{|v|^2}. \tag{18}$$

For the implementation details, please refer to [3, 4].

3.4. Minimizing the Hausdorff Metric

We now explore the relationship between these cost functions and the Hausdorff metric. The Hausdorff metric ***H*** arises in geometric measure theory as a metric between two subsets A, B in R^n defined as

$$H(A,B) = \max(h(A,B), h(B,A));$$
$$h(X,Y) = \max_{x \in X} d(x,Y). \tag{20}$$

Here $d(x, Y)$ is the usual Euclidean distance from the point x to its closest point restricted on the set Y.

Let us re-examine the matching of open curves and modify the cost function by raising the distance functions to some power p and then take the p-th root

$$\min_{a,b,r,\theta}\left(\begin{matrix}\int \{\widetilde{D}_\phi{}^p \delta(\psi_1)\left|\nabla \psi_1\right| H(\psi_2) dx \\ + \int D_\psi{}^p \delta(\widetilde{\phi}_1)\left|\nabla \widetilde{\phi}_1\right| H(\widetilde{\phi}_2) dx\end{matrix}\right)^{1/p}. \tag{21}$$

If we let p go to infinity, the limit of the above cost function is exactly the Hausdorff metric between the two curves. Numerically, we use a p much larger than one to approximate the L infinity norm. Thus, minimizing the Hausdorff metric between geometric objects is natural using this framework. Moreover, this also provides a strong theoretical foundation for our approach.

3.5. Non-rigid feature based warping in computational anatomy

Computational anatomy [5-7] is an emerging new discipline that deals with analyzing large collections of biomedical images. A fundamental problem in computational anatomy is mapping one image dataset to another through a diffeomorphic transformation. The strategy proposed in this paper can be utilized to perform feature based image warping in computational anatomy. We solve for a displacement u at each point x such that under this displacement one image is transformed to the other. Moreover, we model u as the inverse map of the solution of an Euler transport equation with velocity field v

$$x - u(x) = g^{-1}(x,t);$$
$$\frac{\partial}{\partial t} g(x,t) = v(g(x,t),t). \tag{22}$$

For a detailed discussion, we refer the reader to [4, 6].

4. RESULT

To validate our approach, brain MR images from one control subject and an average human brain template as discussed in [6] are used. A template of 3D structural and functional landmark curved lines is delineated on the brain surfaces. Figure 1 shows the brain hemisphere of the normal subject with the identified landmark curves in 3D. The brain surfaces are represented by a spherically-parameterized, triangulated 3D mesh, and thus in the flattened-out parameter space the landmark curves could be easily re-identified. Furthermore, a RGB color code is used to store the original 3D position at each point in the flat parameter space. The landmark based warping is then applied on the parameter space and the deformation is pulled back onto 3D brain surfaces using the color-coded 3D information. Figure 2 shows the flattened brain surface of the control subject before and after warping with the landmark curves overlaid. This transform matches the landmark curves

while smoothly propagating the transform to the rest of the parameter space.

References

[1]S. Osher and J. A. Sethian, "Fronts Propagating with Curvature-Dependent Speed - Algorithms Based on Hamilton-Jacobi Formulations," *Journal of Computational Physics*, vol. 79, pp. 12-49, 1988.

[2]P. Smereka, "Spiral crystal growth," *Physica D*, vol. 138, pp. 282-301, 2000.

[3]N. Paragios, M. Rousson, and V. Ramesh, "Matching Distance Functions: A Shape-to-Area Variational Approach for Global-to-Local Registration," *ECCV*, 2002.

[4]W. H. Liao, "Mathematical techniques in object matching and computational anatomy: a new framework based on the level set method," in *Biomathematics*. Los Angeles: UCLA, 2003.

[5]P. Thompson and A. W. Toga, "A framework for computational anatomy," *Computing and Visualization in Science*, vol. 5, pp. 13-34, 2002.

[6]M. I. Miller, A. Trouve, and L. Younes, "On the metrics and Euler-Lagrange equations of computational anatomy," *Annual Review of Biomedical Engineering*, vol. 4, pp. 375-405, 2002.

[7]U. Grenander and M. I. Miller, "Computational anatomy: An emerging discipline," *Quarterly of Applied Mathematics*, vol. 56, pp. 617-694, 1998.

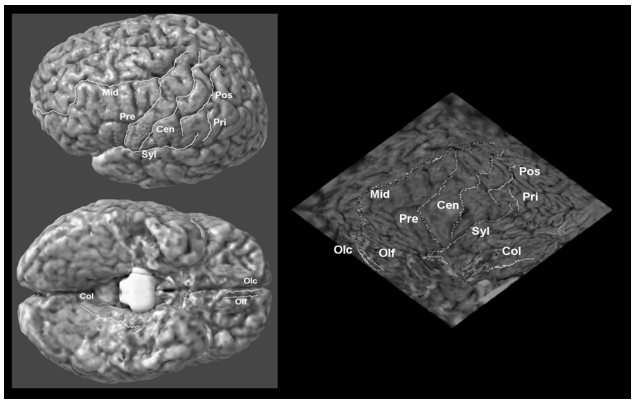

Figure 1. The brain hemisphere of one normal subject with the identified nine landmark sulcal curves used for brain surface matching. Left panel: sulcal delineations on the original 3D brain surface (left hemisphere). Right panel: the surface of the left hemisphere overlaid with the same nine sulcal curves in the flattened parameter space.

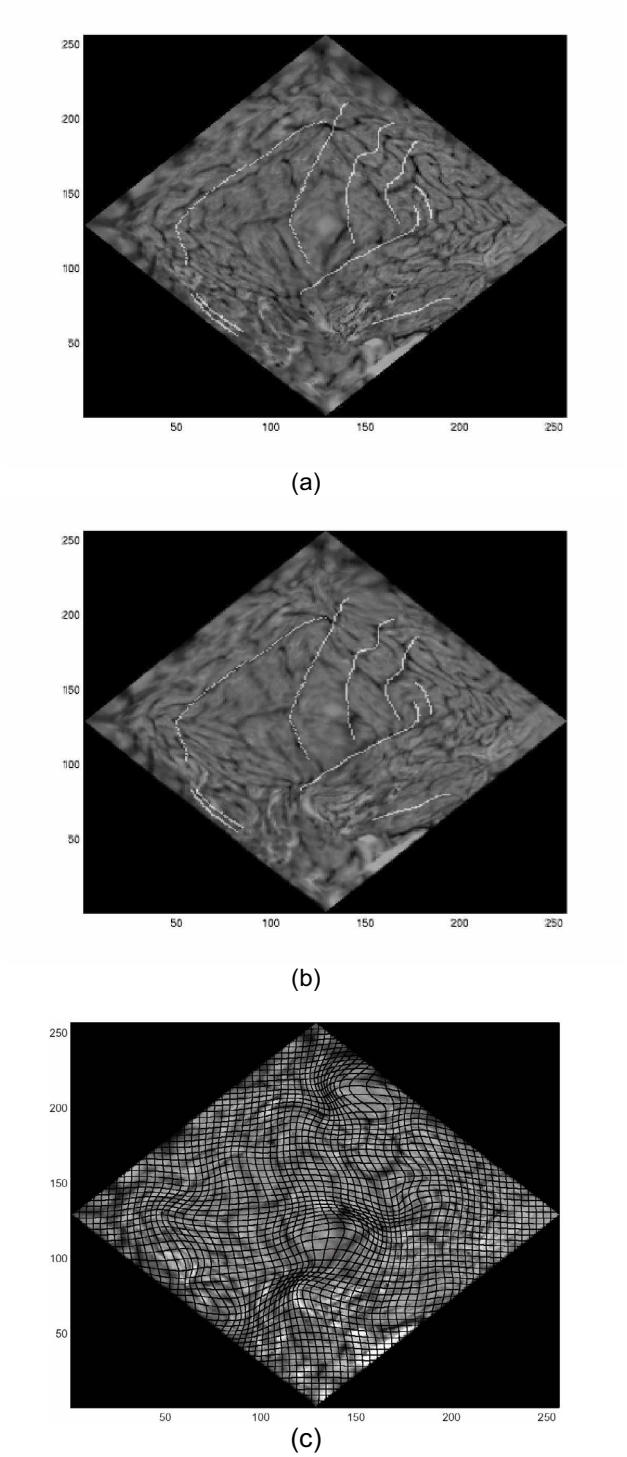

Figure 2. Brain warping using landmark curve matching from the normal subject in Figure 1 to the average human brain: (a) The flattened brain surface overlaid with average landmark curves. (b) Warped brain in (a) overlaid with average landmark curves. (c) Warped brain with grid deformation.